nature photonics

ARTICLES

https://doi.org/10.1038/s41566-018-0135-2

Massively parallel sensing of trace molecules and their isotopologues with broadband subharmonic mid-infrared frequency combs

A. V. Muraviev[1], V. O. Smolski[1,2], Z. E. Loparo[3] and K. L. Vodopyanov[1]*

Mid-infrared spectroscopy offers supreme sensitivity for the detection of trace gases, solids and liquids based on tell-tale vibrational bands specific to this spectral region. Here, we present a new platform for mid-infrared dual-comb Fourier-transform spectroscopy based on a pair of ultra-broadband subharmonic optical parametric oscillators pumped by two phase-locked thulium-fibre combs. Our system provides fast (7 ms for a single interferogram), moving-parts-free, simultaneous acquisition of 350,000 spectral data points, spaced by a 115 MHz intermodal interval over the 3.1–5.5 μm spectral range. Parallel detection of 22 trace molecular species in a gas mixture, including isotopologues containing isotopes such as ^{13}C, ^{18}O, ^{17}O, ^{15}N, ^{34}S, ^{33}S and deuterium, with part-per-billion sensitivity and sub-Doppler resolution is demonstrated. The technique also features absolute optical frequency referencing to an atomic clock, a high degree of mutual coherence between the two mid-infrared combs with a relative comb-tooth linewidth of 25 mHz, coherent averaging and feasibility for kilohertz-scale spectral resolution.

Coherent laser beams provide a unique prospect for sensing molecules through their resonant absorption features—either remotely or via multipass action. A target window for ultrasensitive molecular spectroscopy is the 3 to 20 μm region of the mid-infrared (mid-IR) spectrum, where the strongest absorption lines can be addressed. For example, the sensitivity of the measurement of radiocarbon dioxide ($^{14}CO_2$) concentration, with respect to the main isotopologue ($^{12}CO_2$), down to five parts per quadrillion (5×10^{-15}) has already been demonstrated using mid-IR laser spectroscopy[1]. Frequency combs—manifolds of evenly spaced and phase-locked ultra-narrow spectral lines produced by phase-stabilized femtosecond lasers—were introduced in the late 1990s and have revolutionized accurate measurements of frequency and time[2]. In the mid-IR range, the advent of optical combs brought a new set of tools that substantially improved both the precision and sensitivity of molecular detection[3].

Spectroscopic applications of optical frequency combs include (1) sensing with a broadband comb that directly interrogates an absorbing sample, after which the spectrum is dispersed in two dimensions and sensed with detector arrays[4–6], (2) Michelson interferometer-based Fourier-transform spectroscopy[7–11] and (3) dual-comb spectroscopy (DCS), which is based on superimposing two mutually coherent frequency combs[12–26]. In DCS, a second frequency comb, with a small offset of mode spacing (pulse repetition frequency), effectively plays the role of the time-delayed second arm in the Michelson interferometer. However, the DCS technique requires a high degree of coherence between the two combs, and most studies that have made full use of the advantages of the technique (broad spectral coverage, comb-tooth resolved spectra and rapid scans) have so far been limited to the near-infrared domain[15–17].

The true promise of DCS for sensitive molecular detection lies in the mid-IR. Proof-of-principle demonstrations have been carried out in the 10 μm wavelength region (instantaneous spectral span 250 cm^{-1}, spectral resolution 2 cm^{-1})[13], in the 2.4 μm region (span 200 cm^{-1}, resolution 2 cm^{-1})[18] and in the 3 μm region (150 cm^{-1}, 0.2 cm^{-1} (ref. [19]); 250 cm^{-1}, 0.8 cm^{-1} (ref. [20]); 350 cm^{-1}, 0.2 cm^{-1} (ref. [21]); 250 cm^{-1}, 0.07 cm^{-1} (ref. [22]); 160 cm^{-1}, 0.5 cm^{-1} (ref. [23])). A broadband (2.6–5.2 μm) DCS technique has been reported[24] using combs created via difference frequency generation. However, the above span was covered in several steps, by adjusting the proper poling period of the frequency mixing crystal for each step. Also, very high spectral resolution has been demonstrated in the 3.4 μm region, though with reduced spectral coverage (span 30 cm^{-1}, resolution 10 kHz $\approx 3\times10^{-7}$ cm^{-1})[25], and in the 7 μm region (span 16 cm^{-1}, resolution 0.003 cm^{-1})[26].

For simultaneous detection of an assortment of molecules with different functional groups, one needs a spectrally broad comb, ideally spanning an octave or more. Recently, it has been demonstrated that highly coherent and broad-bandwidth mid-IR combs can be created in a synchronously pumped optical parametric oscillator (OPO) operating at degeneracy, which is also referred to as a divide-by-two subharmonic OPO or half-harmonic generator[27–29], and where the spectrum that spans well above an octave in the mid-IR can be produced[30]. In such a divide-by-two OPO, the output is inherently frequency- and phase-locked to the pump. The relative linewidth between the comb teeth of the pump laser and its subharmonic has been measured to be well below 1 Hz (refs [31,32]).

Here we report on our results with a dual-comb spectrometer that uses a pair of low-threshold broadband subharmonic OPOs with high mutual coherence. We were able to simultaneously obtain 350,000 comb-tooth-resolved data points over the entire spectral range of 3.1 to 5.5 μm (span >1,300 cm^{-1}, resolution <0.0038 cm^{-1}) with the measurement time varying from 7 ms to 1,000 s, and demonstrate parallel detection of numerous molecular species in a mixture of gases.

Results

Dual-comb mid-IR system based on optical subharmonic generation. Our dual-comb mid-IR system starts with two optically referenced phase-locked thulium (Tm)-fibre laser frequency combs that

[1]CREOL, College of Optics and Photonics, University of Central Florida, Orlando, FL, USA. [2]IPG Photonics-Mid-Infrared Lasers, Birmingham, AL, USA. [3]Mechanical and Aerospace Engineering, University of Central Florida, Orlando, FL, USA. *e-mail: vodopyanov@creol.ucf.edu

pump two independent OPOs. The lasers had the following parameters: central wavelength 1.93 µm, repetition rate 115 MHz, pulse duration 90 fs and average power ~300 mW for each laser. To stabilize the frequency comb for each Tm laser, part of the oscillator light was amplified to generate a supercontinuum spanning 1.0–2.3 µm in a nonlinear silica fibre. While the 1.1 µm and 2.2 µm supercontinuum components were used to measure the carrier-envelope offset (CEO) by *f*–2*f* interferometry[31,33], the supercontinuum component near 1.56 µm was used obtain frequency beats with a stable continuous-wave reference diode laser. These two beat frequencies were coherently locked to fixed values, such that the frequency comb teeth had the same linewidth (3 kHz) as the continuous-wave reference (see Methods).

The twin Tm-fibre comb system with an offset of repetition frequencies of $\Delta f_{rep} = 138.5$ Hz pumped two identical broadband subharmonic OPOs. Each OPO (Fig. 1a) had a ring-cavity bow-tie design with low roundtrip group delay dispersion achieved by using low-dispersion mirrors, a thin nonlinear gain crystal (0.5-mm-long orientation-patterned gallium arsenide (OP-GaAs)) and an intracavity CaF_2 wedge for the group-velocity dispersion control. The same wedge was used for the OPO beam outcoupling (see Methods). A low pump threshold of ~10 mW for each of the OPOs was typical for such a doubly resonant system[30]. The instantaneous spectral coverage of our DCS system was 3.14–5.45 µm (1,835–3,185 cm^{-1}) at the −25 dB level, set by the spectral overlap of the two OPOs.

Mode-resolved spectra and mutual coherence. Figure 2a shows the dual-comb spectrometer setup. The beams from the two OPOs with the average power kept below 10 mW in each beam were spatially combined, passed through a multipass gas cell (AMAC-76LW from Aerodyne, 76 m path length, 0.5 l volume) filled with a mixture of gases and sent to a detector (InSb from Kolmar, 77 K, 60 MHz, longwave cut-off 5.6 µm). The detector output was fed into a 16-bit analogue-to-digital converter (AlazarTech, ATS9626). To obtain mode-resolved spectra and evaluate the instantaneous spectral span of our system, we first used an evacuated gas cell (pressure, $p = 10^{-5}$ mbar), so that only the atmospheric gases outside the cell, such as carbon dioxide and water vapour contributed to the spectrum. Streams of data containing multiple sequential interferograms spaced by $1/\Delta f_{rep} = 7.2$ ms, with a time window of up to 43 s, were recorded. To avoid the folding of the dual-comb radiofrequency (RF) spectrum, the analogue-to-digital converter input was low-pass filtered to <50 MHz. No post processing (except for fast Fourier transform (FFT)) of the raw data was performed in our experiments. A typical detector signal is shown in Fig. 2b. The resulting RF spectrum obtained after Fourier transforming the detector signal is depicted in Fig. 2c. The optical frequency (top axis, cm^{-1}) on this plot was retrieved from the RF using equation (10). The zoomed plots in Fig. 2d,e reveal a comb-mode structure with a 138.5 Hz spacing in the RF domain (115.2 MHz optical) and a finesse of ~4,000. Figure 2f shows the dependence of the RF comb-tooth linewidth (at full-width at half-maximum (FWHM)) as a function of the recording time window duration (τ). With a 43-s-long window, we measured a linewidth of 35 mHz, which is close to the time-bandwidth limit. The best fit in Fig. 2f was obtained assuming a linewidth dependence in the form $\sqrt{\Delta f_0^2 + \Delta f_1^2}$, where Δf_0 is an intrinsic linewidth, and $\Delta f_1 \approx 1/\tau$ is a time-bandwidth-limited linewidth. The fit gives $\Delta f_0 = 25$ mHz, which can be viewed as the relative linewidth between the two subharmonic OPOs (the corresponding mutual coherence time is 40 s). Figure 2g shows the comb-tooth-resolved optical spectrum when the gas cell was filled with N_2O at a concentration of 42 ppm in a nitrogen (N_2) buffer gas at a total pressure of 3 mbar. The spectrum reveals single missing comb teeth due to N_2O absorption peaks. Their Doppler linewidth (125 MHz, FWHM) is similar to the intermodal spacing (115 MHz) of our comb. The theoretical N_2O transmission spectrum from the HITRAN database (http://hitran.iao.ru/) is shown at the bottom panel of Fig. 2g.

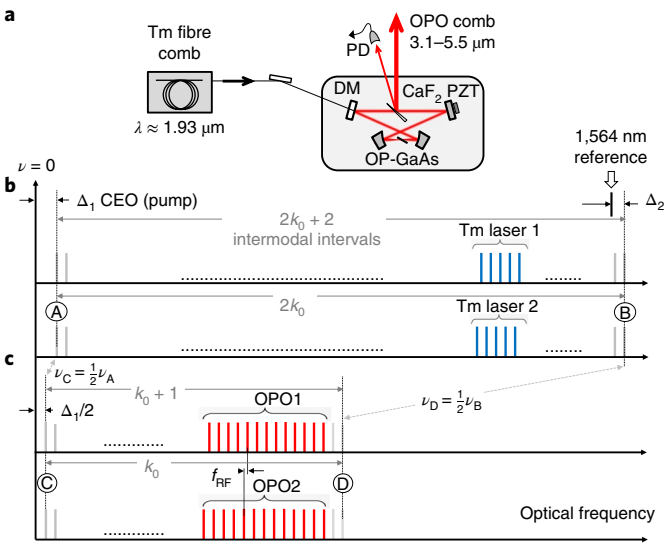

Fig. 1 | Subharmonic OPOs and their comb-mode structure. a, Schematic of an individual subharmonic OPO synchronously pumped by a Tm laser. PD, mid-IR photodetector; DM, dielectric in-coupling mirror; PZT, piezoactuator. **b**, Diagram of comb modes for the two phase-locked Tm-fibre combs. The modes extrapolated to the close-to-zero frequencies (region A) and to the frequency of the continuous-wave 1,564 nm reference laser (region B) are shown in grey. **c**, Comb modes of the two subharmonic OPOs. The OPOs' anchor point C (ν_C) corresponds to half the optical frequency of the lasers' anchor point A (ν_A), and the anchor point D (ν_D) corresponds to half the frequency of the lasers' anchor point B (ν_B) (see Methods).

Measurements with a mixture of gases. To demonstrate parallel spectroscopic detection of multiple species, we filled the optical cell with a mixture of ten molecular gases: N_2O (nitrous oxide) at a concentration of 42 ppm, NO (nitric oxide) at 420 ppm, CO (carbon monoxide) at 120 ppm, OCS (carbonyl sulfide) at 26 ppm, CH_4 (methane) at 1,500 ppm, C_2H_6 (ethane) at 490 ppm, C_2H_4 (ethylene) at 540 ppm, C_2H_2 (acetylene) at 6,600 ppm, CO_2 (carbon dioxide) at 280 ppm and H_2O (water vapour) at 2,100 ppm. The buffer gas was N_2 and the total pressure was 3 mbar. We coherently averaged single DCS interferograms, each with a time window of $1/\Delta f_{rep} = 7.2$ ms, with the total number of averages (N_{ave}) ranging from 100 to 100,000. For each interferogram, the data acquisition process was triggered by a sharp falling edge of the interferogram (Fig. 2b). This can be regarded as an elementary phase correction, as it compensates possible time jitter between interferograms. Such a strategy was feasible due to a very broad spectrum (both optical and RF), resulting in a very sharp negative central peak of the interferogram.

The retrieved DCS spectra are shown in Fig. 3a,b (we did not apply apodization when performing FFT). For a baseline, we used the spectrum taken with the evacuated gas cell (Fig. 3a). Atmospheric gases outside of the cell, mainly carbon dioxide and water vapour, contributed to the dips seen in this spectrum. The 'sample' spectrum—when the optical cell was filled with a mixture of gases (Fig. 3b)—shows characteristic absorption features of different molecules (labelled in Fig. 3b). The two spectra are vertically offset for clarity. Figure 3c–k displays the absorbance spectra $-\ln(T/T_0)$, where T is the transmission of the 'sample' cell and T_0 is that of the evacuated cell, for nine molecules (all except H_2O). Also shown are theoretical spectra from the HITRAN database (inverted in sign) for the given conditions. We observed an excellent matching to HITRAN for all the molecules, in terms of peak

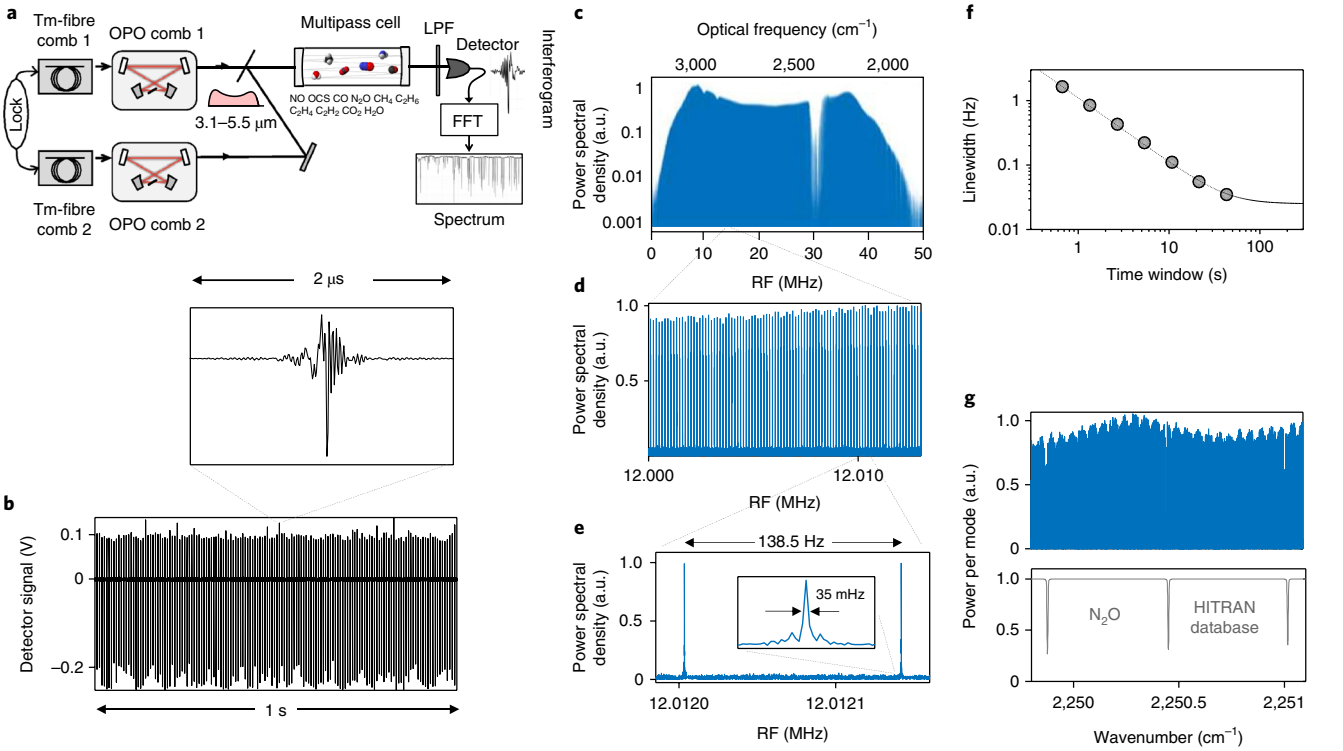

Fig. 2 | Mode-resolved DCS spectra. a, Schematic of the DCS setup. A pair of phase-locked Tm-fibre laser combs pumps a pair of subharmonic OPOs. Their beams are combined, passed through a 76 m multipass gas cell, detected with an InSb detector, digitized and Fourier transformed to retrieve the optical spectrum. A longpass (>2.5 μm) filter (LPF) was used to cut the pump radiation. **b**, Typical detector signal with multiple DCS interferograms recorded over 1 s. **c**, RF spectrum (log scale) obtained via FFT from a single 43-s-long recording. The top scale is the optical frequency retrieved from RF via equation (10). A dip in the spectrum is due to CO_2 absorption in the air. **d**,**e**, Zoomed plots (linear scale) revealing comb-mode structure with 138.5 Hz spacing (115.2 MHz optical) and a finesse of 4,000. The inset shows an individual comb tooth with an RF linewidth of 35 mHz. **f**, Comb-tooth linewidth as a function of recording time. The best fit (dotted line) gives an asymptotic linewidth of 25 mHz. **g**, Comb-tooth-resolved optical spectrum (acquisition time 1 s), which reveals missing modes due to N_2O absorption (top panel). Theoretical N_2O transmission is shown in the bottom panel.

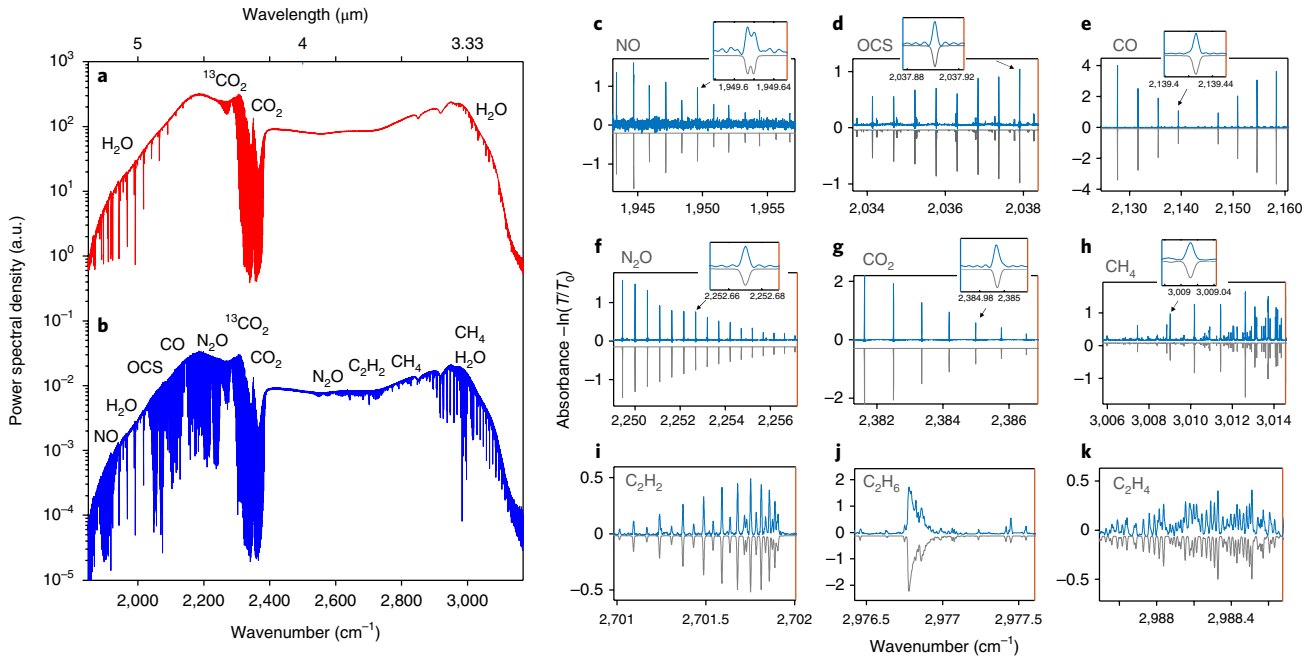

Fig. 3 | DCS spectra of a mixture of gases. a, Optical spectrum (log scale) retrieved from a single coherently averaged interferogram (N_{ave}=100,000) when the gas cell was evacuated. Absorption dips originate from atmospheric gases outside the cell. **b**, Optical spectrum with the gas cell filled with a mixture of ten gases (OCS, N_2O, NO, CO, CH_4, C_2H_6, C_2H_4, C_2H_2, CO_2 and H_2O) in N_2 buffer gas at 3 mbar total pressure. The two curves are vertically offset for clarity. **c**–**k**, Absorbance spectra for nine molecules obtained by normalizing the 'sample' spectrum to that of the vacuum. Theoretical (HITRAN) spectra are also shown (inverted for clarity).

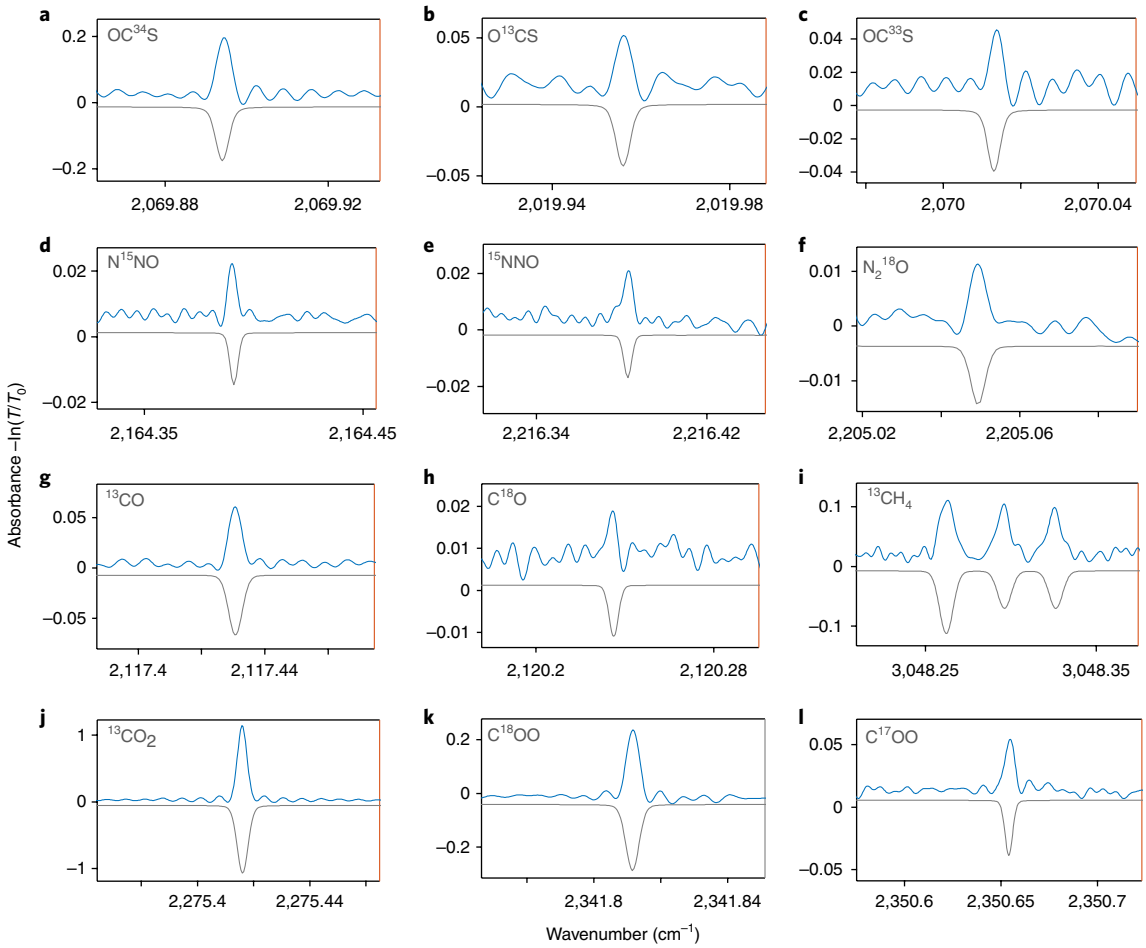

Fig. 4 | Spectra of isotopologues detected in a mixture of gases at 3 mbar. a, $OC^{34}S$. **b**, $O^{13}CS$. **c**, $OC^{33}S$. **d**, $N^{15}NO$. **e**, ^{15}NNO. **f**, $N_2{}^{18}O$. **g**, ^{13}CO. **h**, $C^{18}O$. **i**, $^{13}CH_4$. **j**, $^{13}CO_2$. **k**, $C^{18}OO$. **l**, $C^{17}OO$. Theoretical (HITRAN) absorbance spectra are shown as inverted peaks.

centre (to <1 MHz) and linewidth. In most cases, our spectral sampling (115 MHz) was better than the Doppler-broadened linewidths $\Delta\nu_D^{FWHM}$ of the molecules under study ($\Delta\nu_D^{FWHM}$ varied from 99 MHz for OCS to 283 MHz for CH_4). Some deviations from the HITRAN model, in terms of absorption strength, observed for example in Fig. 3f,j for strong peaks (absorbance >1), we attribute to residual phase error and related pedestals on comb teeth[14]. This phase noise may be caused by time jitter in the data acquisition triggering and can, in general, be eliminated by means of active real-time phase correction[34,35].

With the above mixture of ten molecules, we were able to detect and measure concentrations for twelve of their isotopologues (molecules containing isotopes) that are present in small abundancies, 10^{-2} to 10^{-4} with respect to the main molecule. These include $OC^{34}S$, $O^{13}CS$, $OC^{33}S$, $N^{15}NO$, ^{15}NNO, $N_2{}^{18}O$, ^{13}CO, $C^{18}O$, $^{13}CH4$, $^{13}CO_2$, $C^{18}OO$ and $C^{17}OO$. Figure 4 shows the most prominent absorption peaks for these 12 isotopologues.

Molecular detection in ambient air. In a separate experiment, we measured the DCS spectra of ambient air with a focus on detecting trace molecules and isotopologues. The gas cell was filled with room air at $p = 10$ mbar and single interferograms were coherently averaged. In addition to water and CO_2, we detected and quantified nine other molecules naturally present in the atmosphere in trace amounts, with their spectra shown in Fig. 5. These molecules are: CO at a concentration of 280 ppb, N_2O at 240 ppb, CH_4 at 1.4 ppm, three isotopologues of CO_2 ($^{13}CO_2$, $C^{18}OO$ and $C^{17}OO$) at 3 ppm, 1.3 ppm and 220 ppb, respectively, and three isotopologues of water ($H_2{}^{18}O$, $H_2{}^{17}O$ and HDO (semi-heavy water)) at 160 ppm, 30 ppm and 25 ppm, respectively. With $N_{ave} = 100{,}000$ (12 min recording time), the characteristic peaks of HDO were detected with a signal-to-noise ratio of ~100. For each of the above molecules in air, the concentration was derived via comparison of absorption peaks' strength with the HITRAN simulations.

Noise-equivalent absorbance and detection sensitivity. Figure 6a–c shows absorption spectra of CH_4 (concentration 1,500 ppm, buffer gas N_2 at 3 mbar) at different N_{ave}. Even without averaging (acquisition time 7 ms), one can see the fine structure in the spectrum, corresponding to the Doppler-resolved peaks, including those of the Q-branch around 3,015 cm^{-1}. Figure 6d plots the noise-equivalent absorbance (NEA) as a function of N_{ave}. We define NEA as 3σ, where σ is the relative (with respect to the mean value) standard deviation of the spectral power density in a given spectral region. For example, at $N_{ave} = 100{,}000$, $\sigma \approx 10^{-3}$, which means that we can detect absorption peaks that are 0.3% deep. From Fig. 6d, one can see that NEA scales as $\sqrt{N_{ave}}$, even for large $N_{ave} > 100{,}000$ (measurement time >12 min).

From Fig. 6d and from the HITRAN simulations, it follows that with an acquisition time of 720 s, we can achieve ppb-level sensitivity for species with strong absorption features in the 'flat' portion of our comb, roughly between 2,000 and 3,000 cm^{-1}; namely, we can detect $^{13}CO_2$ at 2 ppb, CO at 11 ppb, OCS at 9 ppb, N_2O at 7 ppb and HDO at 240 ppb concentration. These numbers can be further improved

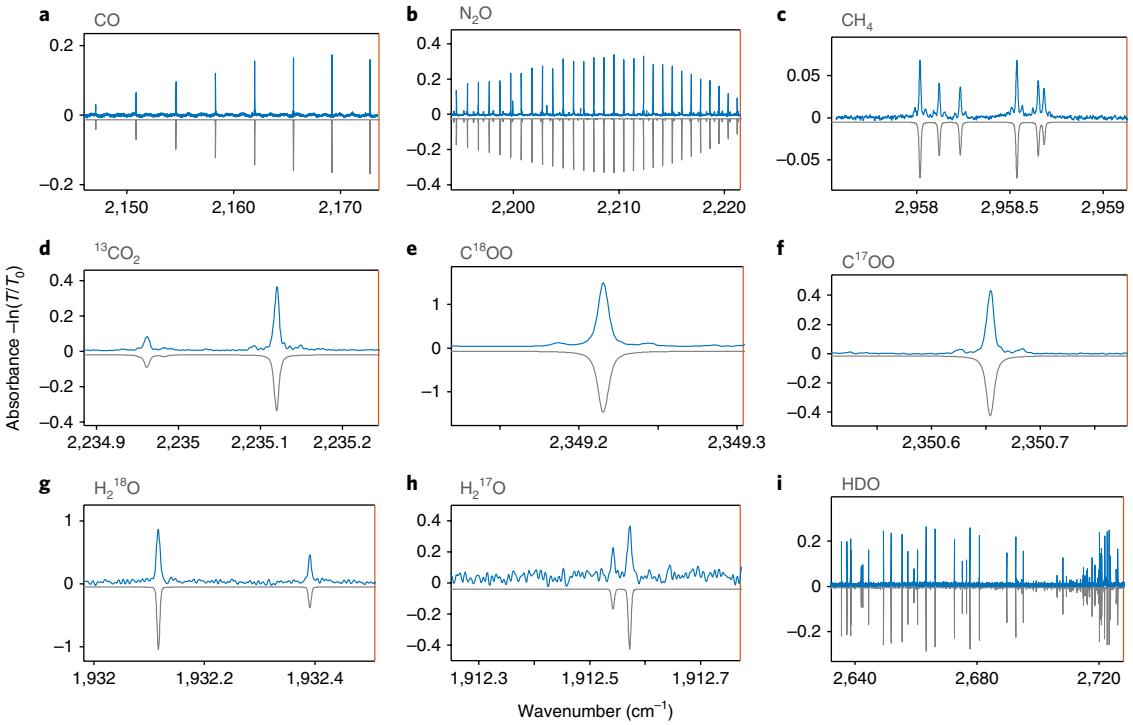

Fig. 5 | Spectra of trace molecules in ambient air at 10 mbar. a, CO. **b**, N_2O. **c**, CH_4. **d**–**f**, Three isotopologues of CO_2. **g**–**i**, Three isotopologues of H_2O. Theoretical (HITRAN) absorbance spectra are shown as inverted peaks.

by a factor of five to ten with the use of a 'matched filter' approach based on the multi-line fitting advantage of broadband DCS[36].

Absolute frequency referencing and resolution limit. Our optical spectra were referenced to RFs only: the frequency counters for measuring f_{rep} and Δf_{rep}, the frequency synthesizers that generated offsets for Tm-fibre combs and the clock of the analog-to-digital (A/D) convertor card were all stabilized against a 10 MHz quartz oscillator locked to a Rb clock (FS725 from Stanford Research Systems). Its absolute accuracy of ~10^{-10} corresponds to ~8 kHz accuracy of the absolute optical referencing. To obtain even higher accuracy, the quartz oscillator can be referenced, for example, to the Cs primary standard via global positioning system.

Finally, in this study, we applied discrete spectroscopic sampling using fixed combs with an intermodal spacing of 115 MHz. Yet, much higher spectral resolution can be obtained in the scanning comb-tooth-resolved mode. We have already demonstrated that by tuning the continuous-wave reference laser, we can scan the comb teeth over the entire intermodal spacing. By interleaving multiple spectra, one can improve the resolution down to the comb intrinsic linewidth. The 25 mHz relative linewidth between our subharmonic combs corresponds to an optical resolution of 25 mHz × $(f_{rep}/\Delta f_{rep}) = 21$ kHz for the full spectral span of 3.1–5.5 μm. By increasing Δf_{rep} by a factor of 10 (at a cost of reducing the full span by the same amount), the resolution can be brought down to ~2 kHz, which is comparable to the absolute comb linewidth of ~3 kHz set by the continuous-wave optical reference.

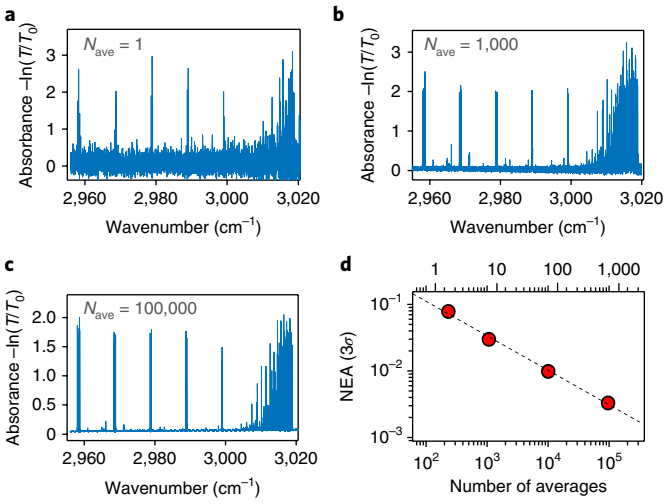

Fig. 6 | Noise and the number of averages. a–**c**, Doppler-resolved spectra for CH_4 for a single interferogram (**a**), for N_{ave} = 1,000 (**b**) and for N_{ave} = 100,000 (**c**). **d**, NEA (at 3σ) as a function of the number of averages. The dashed line is a linear best fit. The top *x* axis is the acquisition time in seconds.

Conclusion

We present a novel approach to DCS in which we use a pair of ultra-broadband (3.1–5.5 μm) subharmonic generators with high mutual coherence. The measurements were performed both in the comb-mode-resolved regime with a continuous recording of multiple interferograms over a time window of >40 s, and by averaging of single interferograms with up to >100,000 interferograms coherently added in real time. In the former case, we resolved comb modes with a finesse of 4,000 and a relative comb-tooth linewidth of 25 mHz, while in the latter case, we acquired 350,000 spectral data points spaced by an intermodal interval (115 MHz) and demonstrated concurrent detection and quantification of up to 22 molecular species, including ones containing isotopes, such as ^{13}C, ^{18}O, ^{17}O, ^{15}N, ^{34}S, ^{33}S and ^{2}H (deuterium), with up to ppb-level sensitivity. We believe our demonstration reveals all the benefits of DCS technique in the mid-IR, including rapid scans, broad spectral coverage, comb-tooth resolved spectra, superior detection capability

and absolute optical frequency referencing. Our DCS platform can be used in various fields, such as medical breath analysis, study of chemical reaction dynamics, atmospheric science and in the search for traces of life in interplanetary missions.

Methods

Methods, including statements of data availability and any associated accession codes and references, are available at https://doi.org/10.1038/s41566-018-0135-2.

Received: 2 October 2017; Accepted: 20 February 2018;
Published online: 26 March 2018

References

1. Galli, I. et al. Spectroscopic detection of radiocarbon dioxide at parts-per-quadrillion sensitivity. *Optica* **3**, 385–388 (2016).
2. Udem, T., Holzwarth, R. & Hänsch, T. W. Optical frequency metrology. *Nature* **416**, 233–237 (2002).
3. Schliesser, A., Picqué, N. & Hänsch, T. W. Mid-infrared frequency combs. *Nat. Photon.* **6**, 440–449 (2012).
4. Diddams, S. A., Hollberg, L. & Mbele, V. Molecular fingerprinting with the resolved modes of a femtosecond laser frequency comb. *Nature* **445**, 627–630 (2007).
5. Nugent-Glandorf, L. et al. Mid-infrared virtually imaged phased array spectrometer for rapid and broadband trace gas detection. *Opt. Lett.* **37**, 3285–3287 (2012).
6. Fleisher, A. J. et al. Mid-infrared time-resolved frequency comb spectroscopy of transient free radicals. *J. Phys. Chem. Lett.* **5**, 2241–2246 (2015).
7. Foltynowicz, A. et al. Optical frequency comb spectroscopy. *Faraday Discuss.* **150**, 23–31 (2011).
8. Haakestad, M. W., Lamour, T. P., Leindecker, N., Marandi, A. & Vodopyanov, K. L. Intracavity trace molecular detection with a broadband mid-IR frequency comb source. *J. Opt. Soc. Am. B* **30**, 631–640 (2013).
9. Meek, S. A., Poisson, A., Guelachvili, G., Hänsch, T. W. & Picqué, N. Fourier transform spectroscopy around 3 μm with a broad difference frequency comb. *Appl. Phys. B* **114**, 573–578 (2014).
10. Khodabakhsh, A. et al. Fourier transform and Vernier spectroscopy using an optical frequency comb at 3–5.4 μm. *Opt. Lett.* **41**, 2541–2544 (2016).
11. Maslowski, P. et al. Surpassing the path-limited resolution of Fourier-transform spectrometry with frequency combs. *Phys. Rev. A* **93**, 021802(R) (2016).
12. Keilmann, F., Gohle, C. & Holzwarth, R. Time-domain mid-infrared frequency-comb spectrometer. *Opt. Lett.* **29**, 1542–1544 (2004).
13. Schliesser, A., Brehm, M., Keilmann, F. & van der Weide, D. W. Frequency-comb infrared spectrometer for rapid, remote chemical sensing. *Opt. Express* **13**, 9029–9038 (2005).
14. Coddington, I., Newbury, N. & Swann, W. Dual-comb spectroscopy. *Optica* **3**, 414–426 (2016).
15. Coddington, I., Swann, W. C. & Newbury, N. R. Coherent multiheterodyne spectroscopy using stabilized optical frequency combs. *Phys. Rev. Lett.* **100**, 013902 (2008).
16. Coddington, I., Swann, W. C. & Newbury, N. R. Time-domain spectroscopy of molecular free-induction decay in the infrared. *Opt. Lett.* **35**, 1395–1397 (2010).
17. Zolot, A. M. et al. Direct-comb molecular spectroscopy with accurate, resolved comb teeth over 43 THz. *Opt. Lett.* **37**, 638–640 (2012).
18. Bernhardt, B. et al. Mid-infrared dual-comb spectroscopy with 2.4 μm Cr^{2+}:ZnSe femtosecond lasers. *Appl. Phys. B* **100**, 3–8 (2010).
19. Zhang, Z., Gardiner, T. & Reid, D. T. Mid-infrared dual-comb spectroscopy with an optical parametric oscillator. *Opt. Lett.* **38**, 3148–3150 (2013).
20. Cruz, F. C. et al. Mid-infrared optical frequency combs based on difference frequency generation for molecular spectroscopy. *Opt. Express* **23**, 26814–26824 (2015).
21. Jin, Y. W., Cristescu, S. M., Harren, F. J. M. & Mandon, J. Femtosecond optical parametric oscillators toward real-time dual-comb spectroscopy. *Appl. Phys. B* **119**, 65–74 (2015).
22. Zhu, F. et al. Mid-infrared dual frequency comb spectroscopy based on fiber lasers for the detection of methane in ambient air. *Laser Phys. Lett.* **12**, 095701 (2015).
23. Kara, O., Zhang, Z., Gardiner, T. & Reid, D. T. Dual-comb mid-infrared spectroscopy with free-running oscillators and absolute optical calibration from a radio-frequency reference. *Opt. Express* **25**, 16072–16082 (2017).
24. Maser, D. L., Ycas, G., Depetri, W. I., Cruz, F. C. & Diddams, S. A. Coherent frequency combs for spectroscopy across the 3–5 μm region. *Appl. Phys. B* **123**, 142 (2017).
25. Baumann, E. et al. Spectroscopy of the methane ν_3 band with an accurate midinfrared coherent dual-comb spectrometer. *Phys. Rev. A* **84**, 062513 (2011).
26. Villares, G., Hugi, A., Blaser, S. & Faist, J. Dual-comb spectroscopy based on quantum cascade laser frequency combs. *Nat. Commun.* **5**, 5192 (2014).
27. Vodopyanov, K. L., Wong, S. T. & Byer, R. L. Infrared frequency comb methods, arrangements and applications. US patent 8,384,990 (2013).
28. Leindecker, N., Marandi, A., Byer, R. L. & Vodopyanov, K. L. Broadband degenerate OPO for mid-infrared frequency comb generation. *Opt. Express* **19**, 6304–6310 (2011).
29. Marandi, A., Leindecker, N., Pervak, V., Byer, R. L. & Vodopyanov, K. L. Coherence properties of a broadband femtosecond mid-IR optical parametric oscillator operating at degeneracy. *Opt. Express* **20**, 7255–7262 (2012).
30. Smolski, V. O., Yang, H., Gorelov, S. D., Schunemann, P. G. & Vodopyanov, K. L. Coherence properties of a 2.6–7.5-μm frequency comb produced as subharmonic of a Tm-fiber laser. *Opt. Lett.* **41**, 1388–1391 (2016).
31. Lee, K. F. et al. Midinfrared frequency combs from coherent supercontinuum in chalcogenide and optical parametric oscillation. *Opt. Lett.* **39**, 2056–2059 (2014).
32. Lee, K. F. et al. Midinfrared frequency comb from self-stable degenerate GaAs optical parametric oscillator. *Opt. Express* **23**, 26596–26603 (2015).
33. Fermann, M. E. & Hartl, I. Ultrafast fibre lasers. *Nat. Photon* **7**, 868–874 (2013).
34. Roy, J., Deschênes, J.-D., Potvin, S. & Genest, J. Continuous real time correction and averaging for frequency comb interferometry. *Opt. Express* **20**, 21932–21939 (2012).
35. Ideguchi, T., Poisson, A., Guelachvili, G., Picqué, N. & Hänsch, T. W. Adaptive real-time dual-comb spectroscopy. *Nat. Commun.* **5**, 3375 (2014).
36. Coddington, I., Swann, W. C. & Newbury, N. R. Coherent dual-comb spectroscopy at high signal-to-noise ratio. *Phys. Rev. A* **82**, 043817 (2010).

Acknowledgements

K.L.V. acknowledges support from the Office of Naval Research (ONR), grant number N00014-15-1-2659 and from the Defense Advanced Research Projects Agency (DARPA), grant number W31P4Q-15-1-0008. Z.E.L. acknowledges support from the National Science Foundation under Graduate Research Fellowship Program, grant number 1144246. We thank J. Jiang and K. Lee for sharing their expertise on the Tm-fibre frequency combs, and N. Newbury and S. Diddams for stimulating discussions.

Author contributions

A.V.M. and V.O.S. constructed the experimental setup. A.V.M. carried out the measurements and analysed the data. Z.E.L. developed the algorithm for data acquisition and processing. K.L.V. initiated and supervised the project; he also analysed the data and wrote the paper.

Competing interests

The authors declare no competing interests.

Additional information

Reprints and permissions information is available at www.nature.com/reprints.

Correspondence and requests for materials should be addressed to K.V.

Publisher's note: Springer Nature remains neutral with regard to jurisdictional claims in published maps and institutional affiliations.

Methods

Optical subharmonic generators. The two low-threshold subharmonic OPOs were synchronously pumped by a pair of phase-locked femtosecond 1.93 μm Tm-fibre lasers (IMRA America). The design for each of the two OPOs (Fig. 1a) copies the one described in detail in ref. [30]. The OPO bow-tie ring cavity was entirely composed of high-reflectivity gold-coated mirrors, except for one in-coupling dielectric mirror with high transmission for the 1.93 μm pump and high reflection in the 3.1–5.7 μm range. (Two extra pairs of gold-coated folding mirrors were used to reduce the footprint and are not shown in Fig. 1a.) The nonlinear gain crystal was a 0.5-mm-long quasi-phase-matched OP-GaAs with a 51.5 μm domain reversal period, designed for subharmonic generation from the 1.93 μm pump. The crystal was placed at the Brewster's angle (73°). A 0.7-mm-thick wedged (1°) CaF_2 plate was used inside the OPO cavity to (1) compensate and fine tune the group delay dispersion and (2) outcouple the OPO power via Fresnel reflection from its two uncoated surfaces. The cavity was purged by dry nitrogen. Because of double (signal and idler) resonance, the OPO is interferometrically sensitive to the cavity-length detuning. We actively locked each OPO cavity to one of its resonances using the 'dither-and-lock' method[28]: the cavity length was dithered using a piezoelectric actuator (PZT) with a small (0.1–1.0 nm) amplitude at ~50 kHz. This modulated the OPO output power seen by a mid-IR photodetector (Fig. 1a); phase-sensitive detection of its output allowed us to generate an error signal, which was fed back to the PZT, such that the cavity length was locked with a servo control bandwidth of ~1 kHz. In this regime, each OPO generated a stable and flat broadband output spanning 3.1–5.5 μm at the −25 dB level. The output power (sum of two beams) for each OPO could be adjusted from a few mW to ~70 mW by varying the angle of the intracavity CaF_2 wedge.

OPO comb modes and RF-to-optical frequency conversion. The comb modes for both Tm-fibre pump lasers were locked at the two common anchor points (Fig. 1b): near zero frequency (via f-to-$2f$ beat note) with a CEO of $\Delta_1 = +190$ MHz (point A), and near the frequency of a common narrow-linewidth (~3 kHz) continuous-wave reference laser at $\lambda \approx 1{,}563.886$ nm with an offset $\Delta_2 = +140$ MHz (point B). Between A and B, there are N_1 intermodal intervals (f_{rep1}) for Tm laser 1 and N_2 intervals (f_{rep2}) for Tm laser 2, such that $N_1 \times f_{rep1} = N_2 \times f_{rep2}$. One can write:

$$\Delta f_{rep} = f_{rep2} - f_{rep1} = \frac{N_1 - N_2}{N_2} f_{rep1} = \frac{\Delta N}{N_2} f_{rep1} = \frac{\Delta N}{N_1} f_{rep2} \quad (1)$$

The repetition rate offset (Δf_{rep}) between the two lasers is therefore quantized, because $\Delta N = N_1 - N_2$ can only take integer values. In our experiments, we used $\Delta N = 2$, such that $\Delta f_{rep} \approx 138.5$ Hz and the dual-comb interferogram appeared every 7.2 ms. One consequence of equation (1) is that for $\Delta N = 2$ and even $N_2 = 2k_0$ and $N_1 = 2k_0 + 2$ (k_0 is an integer), both ratios $f_{rep1}/\Delta f_{rep}$ and $f_{rep2}/\Delta f_{rep}$ are integer numbers. This was used as a test for the accuracy of our frequency counters; in all our experiments, the ratio $f_{rep1}/\Delta f_{rep}$ ($\approx k_0$) appeared as an integer: 831,844 with a deviation <0.001.

The two OPOs were both running in the frequency-divide-by-two mode[30], such that the CEO frequency for each of them was half of that of the pump:

$$f_{CEO}^{OPO1} = f_{CEO}^{OPO2} = \frac{1}{2} f_{CEO}^{pump} = \Delta_1/2 \quad (2)$$

In such a case, the common low-frequency anchor point C (Fig. 1b,c) for both OPOs corresponds to the $\Delta_1/2 = 95$ MHz offset from zero optical frequency. It is important that the numbers N_1 and N_2 are even, as this results in having another anchor point D (near 3.13 μm, twice the wavelength of the continuous-wave reference) for mode numbers $k_0 + 1$ for OPO1 and k_0 for OPO2 (Fig. 1b,c). This ensures that the interferogram reproduces itself for each subsequent event[17].

For OPO1 the comb spectrum can be written in the form (m is the mode number):

$$\nu_{1m} = \Delta_1/2 + m f_{rep1} \quad (3)$$

while for OPO2 the comb spectrum is:

$$\nu_{2m} = \Delta_1/2 + m f_{rep2} \quad (4)$$

According to the DCS method[13], the optical spectrum is mapped to the RF spectrum obtained by taking a FFT of the interferogram acquired from a mid-IR detector. From equations (3) and (4), it follows that the RF comb line corresponding to the beat note between the two modes with the same number m for OPO1 and OPO2 (assuming $f_{rep2} > f_{rep1}$):

$$f_m = \nu_{2m} - \nu_{1m} = m\Delta f_{rep} \quad (5)$$

probes the optical frequency (ν_m), that is, the mean of ν_{1m} and ν_{2m}:

$$\nu_m = (\nu_{1m} + \nu_{2m})/2 = \Delta_1/2 + m < f_{rep} > \quad (6)$$

where $< f_{rep} > = (f_{rep1} + f_{rep2})/2$ is the average repetition rate. Omitting the indices from the average optical frequency (ν) and RF beat frequency (f), and replacing $< f_{rep} >$ with simply f_{rep}, we get the usual RF-to-optical conversion formula:

$$\nu = \Delta_1/2 + \frac{f_{rep}}{\Delta f_{rep}} f \quad (7)$$

with the term $f_{rep}/\Delta f_{rep}$ playing the role of an up-scaling factor.

For our spectral range of interest (3.14–5.45 μm) and $\Delta f_{rep} \approx 138.5$ Hz, equation (7) brings us to the RF frequency range of 66–115 MHz, which falls between $f_{rep}/2$ and f_{rep}. It is more convenient, however, to look at the 'mirror' image of the RF spectrum, which corresponds to the beat note between the mode number $m+1$ of OPO1 and the mode number m of the OPO2. In this case:

$$f_m = \nu_{1,m+1} - \nu_{2,m} = (m+1) f_{rep1} - m f_{rep2} = < f_{rep} > - \left(m + \frac{1}{2}\right) \Delta f_{rep} \quad (8)$$

The corresponding mean optical frequency ν_m is:

$$\nu_m = (\nu_{1m+1} + \nu_{2m})/2 = \Delta_1/2 + \left(m + \frac{1}{2}\right) \Delta f_{rep} - \frac{\Delta f_{rep}}{4}, \quad (9)$$

From equations (8) and (9), we get the RF-to-optical conversion formula:

$$\nu = \Delta_1/2 + \frac{f_{rep}}{\Delta f_{rep}} (f - f_{rep}) - \frac{\Delta f_{rep}}{4} \quad (10)$$

with the last term (~35 Hz) being small, compared with optical frequencies. The whole 3.14–5.45 μm spectrum is now mapped to the RF range of 0.4–49 MHz, which matches the response of our mid-IR detector (0.01–60 MHz).

Data availability. The data that support the plots within this paper and other findings of this study are available from the corresponding author upon reasonable request.